

APPENDIX 2:

THE MOVEMENT AND DECAY OF ICE EDGE BANDS  
IN THE WINTER BERING SEA

by

**Seelye Martin** and **Peter Kauffman**

**School of Oceanography  
University of Washington**

and

**Claire Parkinson**

NASA/Goddard Space Flight Center

Submitted to Journal of Geophysical Research

April 1982

TABLE OF CONTENTS

Abstract ..... 83

1. Introduction ..... 83

2. How the Buoys Work ..... 85

3. Description of the Band Experiment ..... 88

4. Wave Erosion of the Band ..... 99

5. Stress Balance on the Band ..... 106

6. Concluding Remarks ..... 121

Acknowledgments ..... 121

References ..... 124

## LIST OF FIGURES

- Figure 1. A schematic drawing of the radar transponder buoy. See text for additional description.
- Figure 2. The radar transponder buoy deployed on a floe in the pack ice with the SURVEYOR in background.
- Figure 3. The ship track and buoy deployment for the band experiment. The numbers in parentheses show Greenwich Mean Time on 7 March; the plot is uncorrected for relative ice motion except for the relative position of JAREL to KURT which was determined at 2305 from the radar.
- Figure 4. A schematic drawing of the band appearance on 9 March 1981, 0000 GMT. Except for the radar-derived distance between the buoys, the sketch is qualitative. The arrows show the direction of buoy motions; the symbol shows the ship position.
- Figure 5. A composite photograph of the band made at the same time as Figure 4. The ship is downwind of the band; the arrows mark the approximate buoy positions.
- Figure 6. The buoy trajectories over the entire deployment period. The last point on 'KURT' is from the ship's log, not our records. See text for additional description.
- Figure 7. The relative separation and angle between the two buoys. The vertical arrow on the upper curve marks the logged melt-out time for KURT; the times are in Julian days and hours, where day 67 is 8 March.
- Figure 8. A schematic drawing of the ice features encountered during the return to the ice edge on 10 March, 0100 - 0400 GMT. The solid line shows the cruise trajectory; the adjacent numbers give times in GMT; the numbers in parentheses are the water temperatures in degrees. The arrow shows the mean wind direction; the mean wind speed was  $15 \text{ m s}^{-1}$ .
- Figure 9. Relative displacement of KURT from Pease's station. The dots show the separation, the solid straight line is a least-squares fit showing that KURT moved away from Pease's station at a speed of  $0.48 \text{ km hr}^{-1}$  or  $0.13 \text{ m s}^{-1}$ .
- Figure 10. Composite photograph of a small 100 m wide band; downwind is to the left, upwind is to the right.

- Figure 11. Schematic drawing in cross-section of the evolution of a band in a wave field. (a) Initial band configuration; (b) some time later. See text for additional discussion
- Figure 12. Seawater temperature versus time for the band experiment
- Figure 13. Details of an upwind band edge, following 9 March 0000 GMT. (a) The upwind edge; (b) the floes behind the band; (c) small floes melting in open water. See text for further description.
- Figure 14. A chart of the experimental region. The point 'BC22' shows the current meter position; the line 'a' shows the net translation of Pease's station for the times shown at the endpoints; line 'b' shows the net band translation. The numbers in parentheses under the times are water temperatures in degrees.
- Figure 15. Comparison of the band velocity with the currents measured at **BC22**. The upper two curves show the east  $u_C$  and north  $v_C$  current components from **BC22**; the middle two curves show the ice band components  $u_I$  and  $v_I$ ; the lower two curves show the relative velocities  $u_R$  and  $v_R$ . See text for additional description.
- Figure 16. Observed wind speed and direction for the band experiment as measured on the ship at one-hour intervals
- Figure 17. Sketch of ice band made on 11 March 0400 GMT while leaving the ice edge (courtesy Scott **Ferguson**).

## LIST OF TABLES

- Table 1. Average velocities used in the calculation of "the ice momentum balance.
- Table 2. Stresses on the ice band.
- Table 3. Stress balance at Pease's station.
- Table 4. Recalculation of the stress balance on the ice band, using Pease's water stress scaled up from Table 3.
- Table 5. Radiation stress ( $\text{N m}^{-1}$ ) and resultant band widths (m) as a function of Fetch X, and windspeed  $U_{10}$ .

## ABSTRACT

During periods of off-ice winds, the winter Bering Sea ice edge consists of ice bands which measure 1 - 10 km in length, 0.1 - 1 km in width, and are oriented at approximately right angles to the wind. The bands are made up of small floes 10 - 20 m in diameter and 1 - 5 m in thickness. In March 1981 working from the NOAA ship SURVEYOR, we mounted two radar transponders 4 km apart on such a band, then tracked them for 46 hr over an 80 km distance as the band moved into warmer water and melted. Comparison of the band position with that of a satellite-tracked ARGOS station deployed in the ice interior shows that the band moved 30% faster than the interior ice. Both our observations and analysis strongly suggest that the cause of this speed increase is the wind-wave radiation stress on the upwind side of the band. We also observed that wind-waves contribute to band ablation by the following mechanism: At the upwind edge, these waves break up the floes into small pieces. Because these pieces are no longer good wave reflectors or absorbers, they drift relatively upwind to melt, so that the band width, as well as the individual floe thicknesses, decrease with time. In summary, because the bands provide an efficient way for the export and ablation of sea ice, the bands play a major role in the maintenance of the ice edge position.

1. Introduction

At the winter Bering Sea ice edge during periods of off-ice winds, the pack ice forms into long bands of **ice** measuring 1 - 10 km in length, and 0.1 - 1 km in width, with their long axes at right angles to the wind. After formation, these long bands move away from the interior ice and **melt** in the warmer southerly waters.

From a satellite study, **Muench** and **Charnell** (1977) show that these bands extend over a 50 - 100 km distance downwind of the pack ice, and have a regular spacing in the wind direction of 6 - 12 km. In a subsequent field study, **Bauer** and **Martin** (1980) show that the ice which makes up the bands comes from the outer 5 - 10 km of the pack ice, and consists of small thick floes measuring approximately 10 - 20 m in diameter, and **1 - 5 m in thickness**. The reason these **floes** occur is that the propagation of ocean **swell** into the pack fractures, rafts, and ridges the large interior floes into the observed small floes. **Bauer** and **Martin** also observed from the tracking of **visual** targets in a band, that the band moved southwest at the higher velocity than the originally adjacent pack ice; they attribute this speed increase to the wind-wave radiation stress generated in the fetch between the band and the pack ice acting on the upwind side of the band.

The present paper describes a study of the movement and decay of these bands carried out in March 1981 from the **NOAA** ship SURVEYOR. In this study, we tracked a pair of radar transponders mounted on **ice** floes within a band. We also compared the band motion to that of a satellite-tracked buoy deployed by **Pease** (1982) in the ice interior. The study showed the following: first, that the bands moved away from the interior pack ice at speed 30% greater than that of the

interior ice; second, that the cause of this band acceleration was very likely the wind-wave radiation stress on the upwind side of the band; third, that as the bands moved into warmer water, they decayed both by wind-wave erosion of the upwind edge and by bottom melting.

In the following, Section 2 describes how the buoys work and our method of deployment. Then, Section 3 describes the band shape and trajectory, and Section 4 describes how the band decays. Finally, Section 5, through a calculation of the steady state stress balance on the band, shows that the radiation stress can account for the velocity increase of the band relative to the ice interior.

## 2. How the Buoys Work

Figure 1 is a schematic drawing of the radar transponder buoy, and Figure 2 is a photograph of a buoy deployed in an ice **floe**. We built these buoys from 3 m lengths of PVC pipe with an 8 mm wall thickness and a 0.17 m outer diameter. The pipes, which were sealed at the top and bottom with stock end caps, fitted into a standard 0.2 m diameter auger hole. We designed the buoys both to transmit from the **ice** and to **float** upright in and transmit from open water. So that the buoy fulfilled both these functions, inside the tube we mounted the radar transponder at the top with a timing circuit just beneath it, additional flotation in case of leaks in the middle, and the batteries at the bottom. Outside of the tube we fastened styrofoam flotation around the middle, and suspended 17 kg of chain from the tube bottom. This allowed the buoy to float upright in open water with 1.3 m of freeboard. We also fasterted a wire harness above and below the flotation to which we attached a 50' length of 3/8" polypropylene line looped through a VINYL-FLOAT . This line and float allowed us to recover the buoy from open water with a grappling hook. The transponder had a current consumption of 0.5 amps, and the lead-acid batteries had a 10 **amp-hr** lifetime. Therefore to stretch our

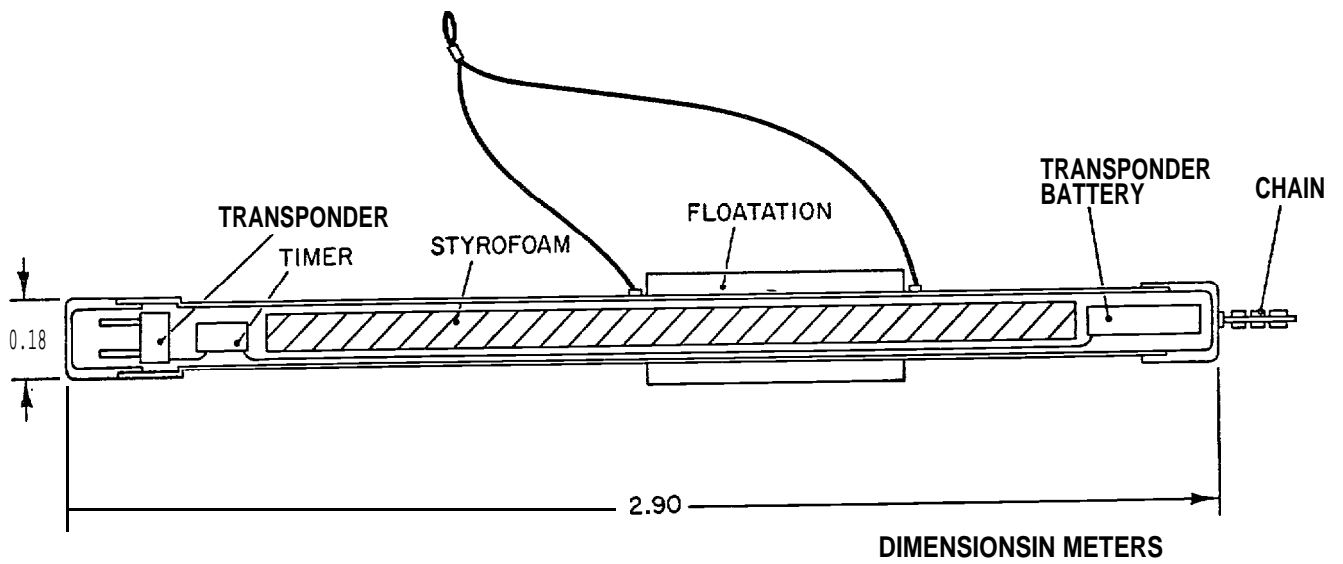


Figure 1. A schematic drawing of the radar transponder buoy. See text for additional description.

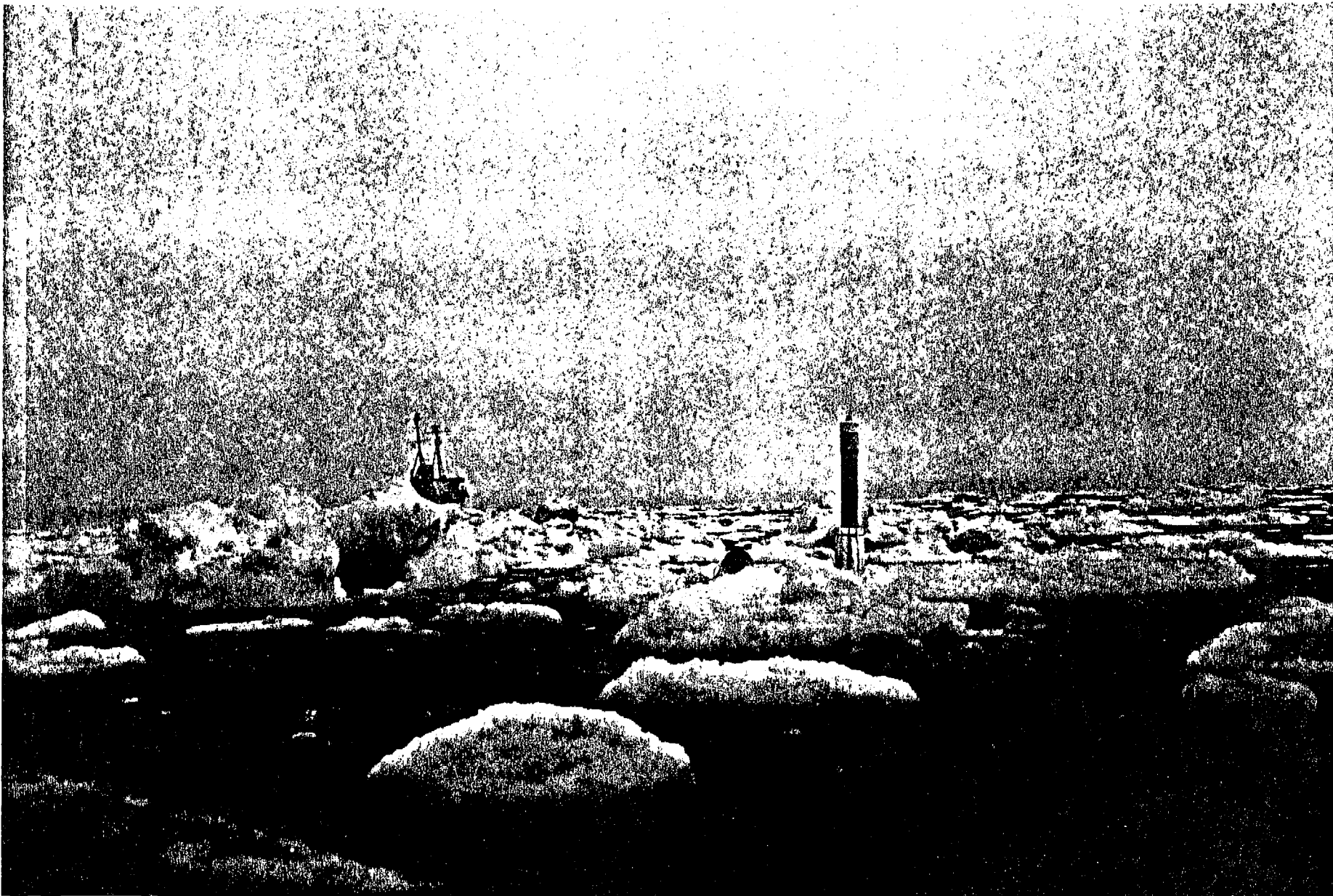


Figure 2. The radar transponder buoy deployed on a floe in the pack ice with the SURVEYOR in background.

operational time to 60 hr, we added the timer shown on Figure 1 below the transponder, which turned the transponder on for one minute, then off for two.

To install the buoy on an ice floe, we tied the ship against a suitable floe, went down on the ice, cored an auger hole, dropped the buoy in this hole, and attached the VINY-FLOAT. The entire procedure took about 1 hr. Once the buoys were deployed, we tracked them with the X-Band radar on the ship. We then recorded their range and bearing from the radar and the ship's position from the Loran-C at 0.5 hr intervals. We estimate that our position accuracy from the radar was about  $1^\circ$  in bearing, and 100 m in range. Off the ship, we reduced the data to absolute buoy position, which we estimate is accurate to within 100 m.

### 3. Description of the Band Experiment

In the experiment, we deployed the two buoys, named 'KURT' and 'JERAL' after two crew members, from the ship around 1200 local time (2200 GMT) on 7 March 1981 along a north-south line about 4 km apart. We deployed the buoys within the outer-most pack ice; Figure 3 shows the approximate ice appearance during the deployment as seen from the ship. Although the SURVEYOR was equipped with a helicopter, a combination of fog, high winds, and rotor icing prohibited our flying and viewing the ice from above throughout the band study.

In the deployment region, the ice consisted of floes with diameters ranging from 1 - 15 m. The floe **JERAL** was about 5 m in diameter and 1.2 m thick; the floe **KURT** was about 6 m in diameter and again 1.2 m thick. The maximum pressure ridge height within the region was about 1 m, which implies a ice keel depth of about 5 m. As Figure 3 shows, initially the ice containing the buoys did not appear to be a band; rather it had a north-south length scale greater than 6 km, and an east-west scale of order 1 - 2 km. Following deployment the ice advanced southwest in response to the  $10 \text{ m s}^{-1}$  northeast winds.

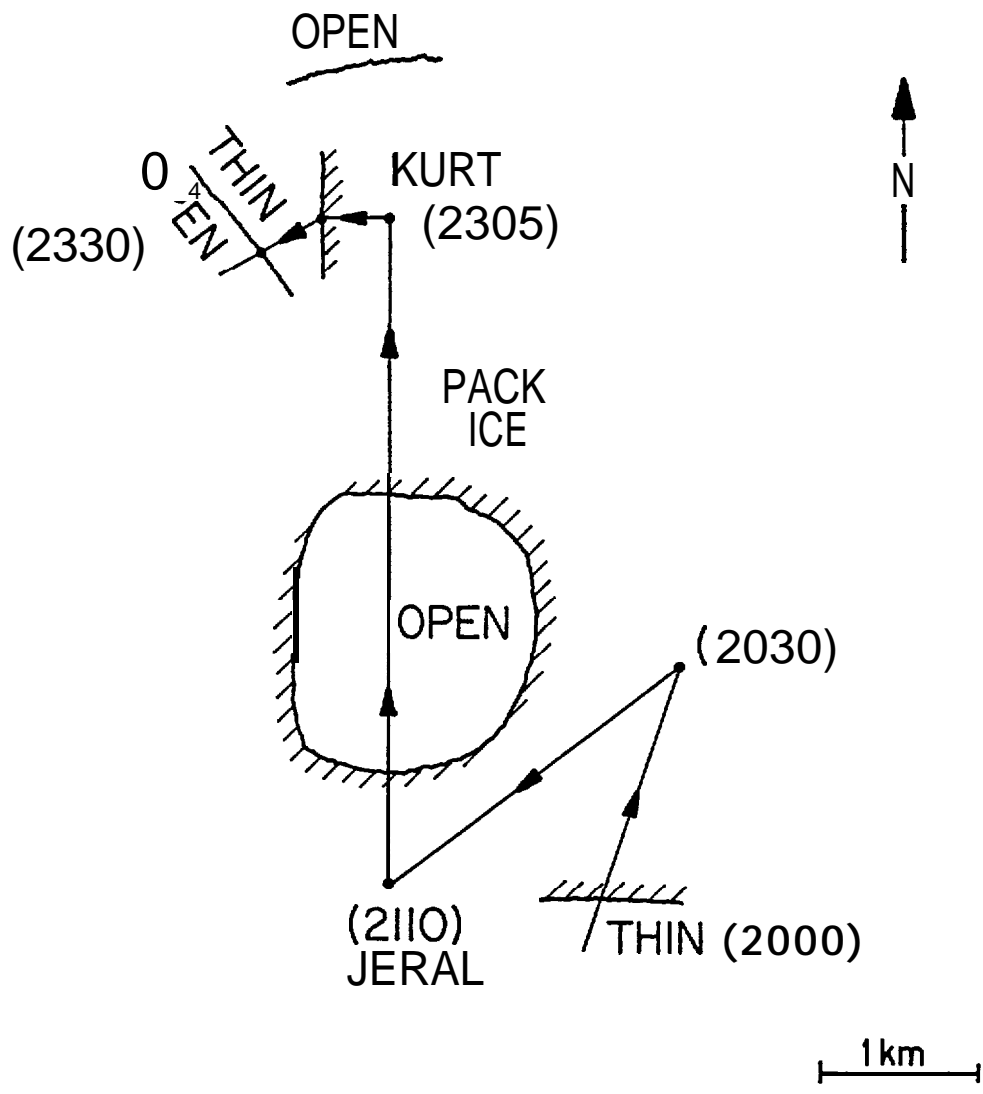


Figure 3. The ship track and buoy deployment for the-band experiment. The numbers in parentheses show Greenwich Mean Time on 7 March: the plot is uncorrected for relative ice motion except for **the** relative position of JAREL to KURT which was determined at 2305 from the radar.

The following day, the wind velocity remained from the northeast and increased to  $20 \text{ m s}^{-1}$ . To show that the ice floes were now organized into a band, Figure 4 shows a sketch of the band appearance made from the ship on 9 March, 0000 GMT; and Figure 5 shows a composite photograph made at the same time with arrows indicating the approximate buoy positions. As the figures show, the band was long and narrow with a curve in the middle; the band maintained this appearance throughout the day. To avoid disturbance of the band, we deliberately kept the ship downwind and at least a km away. We continued tracking the band through the evening of 8 March, while the northeast wind velocity remained high. At 0230 **local**, we noted that KURT was not **transponding** regularly; at 0530, **JERAL** stopped **transponding** completely. At 0630, the ship moved against the ice band to take a CTD observation, at which time KURT was weakly **transponding** 1.5 km away to the northeast.

Therefore, at first light we decided to recover KURT; we steamed through the band which was now no more than 50 m wide, and picked up KURT at 0830 **local** in open water well upwind of the band. At pick-up, we found that the flotation collar on KURT had slipped upward so that **it** was adjacent to the, expansion section at the top of the buoy. This lower buoy freeboard explained the **signal** attenuation. We then steamed on a dead-reckoning course for JAREL, and picked it up at 0900 local, again well away from any ice. The flotation had not slipped on JAREL; however, the high winds had blown the hull over so that the buoy lay nearly horizontal in the water. Because of this, we assumed that JAREL ceased **transponding** after breaking out of the ice.

The buoy trajectories for the entire 46 **hr** deployment are shown in Figure 6. The upper curve shows buoy KURT; the **lower** curve, **JAREL**. The dots on the curves show our position fixes at 0.5 hr intervals. The broken vertical arrows between the two trajectories show the position and relative orientation of the **two** buoys at 6

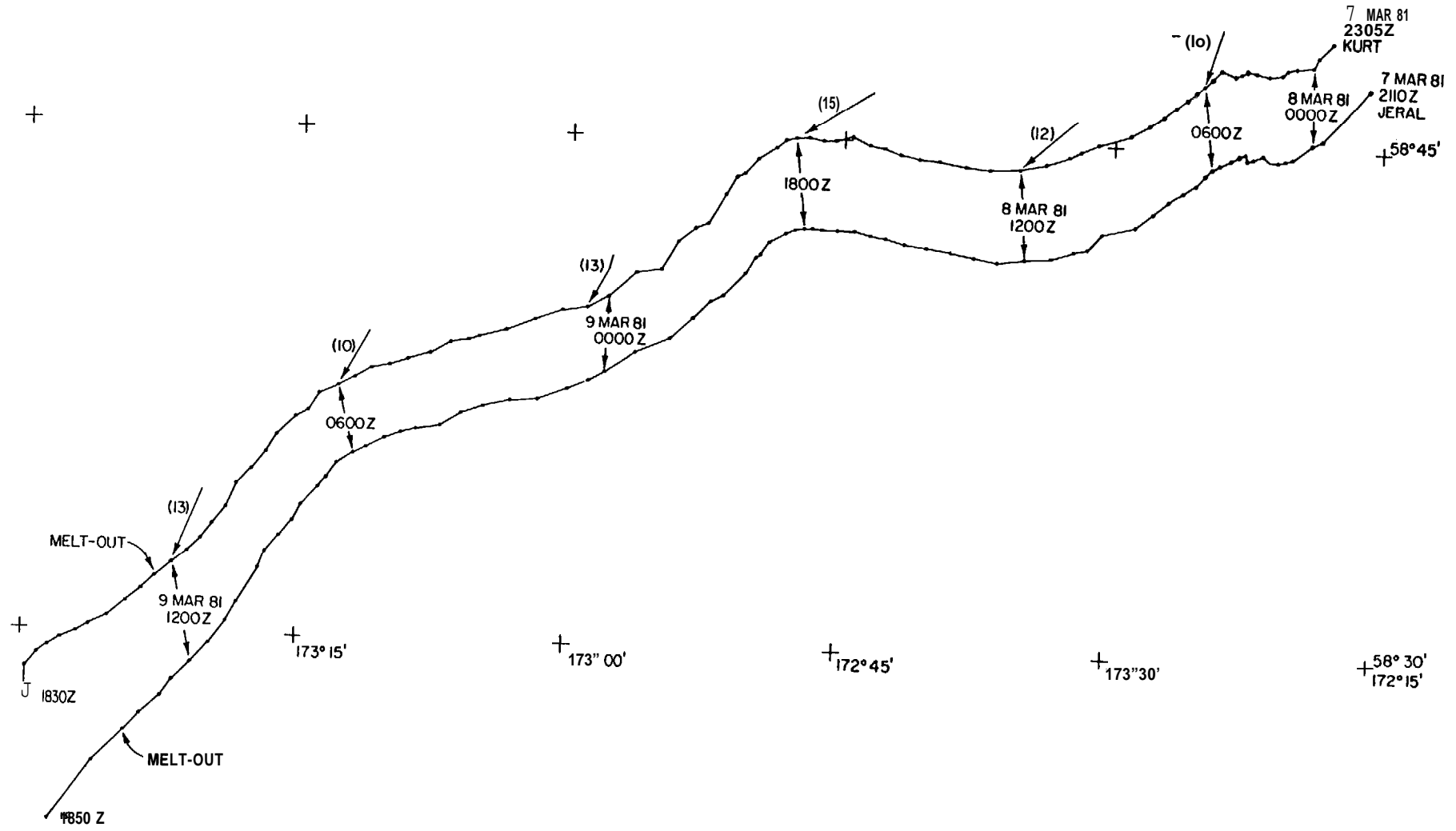


Figure 6. The buoy trajectories over the entire deployment period. The last point on 'KURT' is from the ship's log, not our records. See text for additional description.

hr intervals for the times listed in GMT in the arrow gaps. The sloping arrows above the trajectories show the wind direction; the numbers in parentheses beside the arrows show the wind velocity in  $\text{m s}^{-1}$ . Finally, the points labeled 'melt-out' are where we observed the transponder signal strength to diminish. The figure shows that over the deployment period, the wind advected the buoys to the west, with a mean speed of about  $2 \text{ km hr}^{-1}$ . The figure also shows the oscillations on the trajectories caused by the diurnal and semi-diurnal tides discussed below and that the buoys maintained approximately the same orientation and distance apart.

To discuss the relative positions of the two buoys in more detail, **Figure 7** is a plot of buoy separation and angle versus time. Our original hypothesis for the reason that the bands became thinner **as** they moved downwind was that the incident ocean swell caused them to stretch out in length. Both Figures 6 and 7 however, clearly show that before the transponders melted out of the ice, the distance between them only varied between 4 and 5 **km** and their relative angle remained between  $340^\circ$ - $360^\circ$ . In addition, Figure 7 shows that before melt-out, **as** the band moved west, it neither appreciably stretched nor rotated, **while** after melt-out the buoys diverged rapidly. As we will show below, the cause of the band growing thinner as it moved downwind was wave erosion of the upwind edge.

Next, in order to compare the band velocity with that of the ice interior, we use data from a station deployed by Pease (1982) in the pack ice interior approximately 100 km upwind of the band. At her station, Pease measured position from a satellite-tracked ARGOS buoy, the air stress from an anemometer mast, and the water stress from a current meter suspended 3 m **below** the ice. From her measurements, we are able to compare both the relative velocities of and the stresses acting **on** the band and the ice interior.

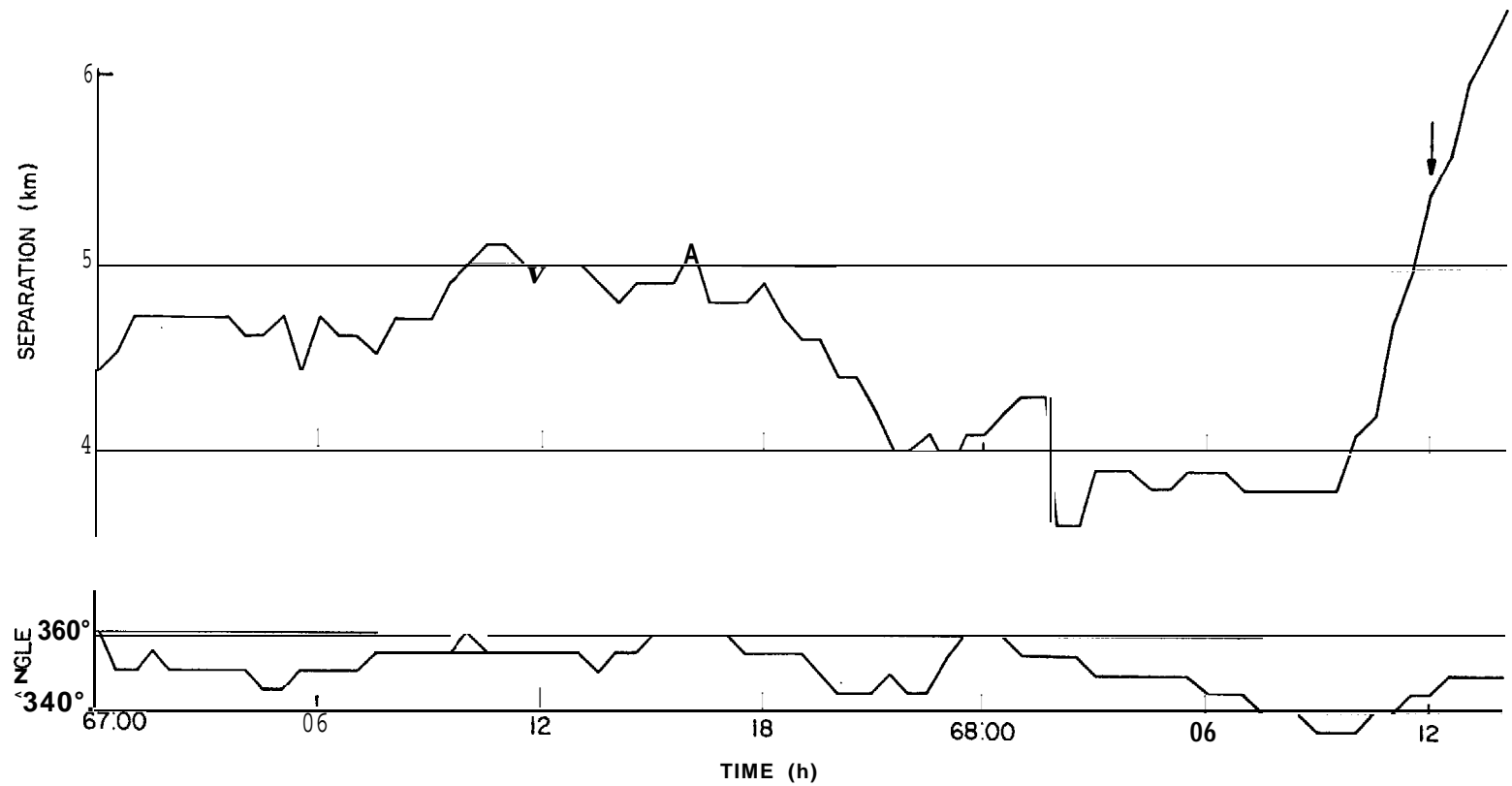


Figure 7. The relative separation and angle between the two buoys. The vertical arrow on the upper curve marks the logged melt-out time for KURT: the times are in Julian days and hours, where day 67 is 8 March.

Before comparison of the band and station velocities, we first describe the ice which lay between the band and Pease's interior station. In the local afternoon of 9 March, after recovery of a meteorological buoy in open water south of our band, we returned to the ice edge to recover Pease's station. Figure 8 shows a sketch of the ice features encountered along the cruise track, where the ship traveled 37 km over the 3 hr period 0100-0400 GMT, 10 March. During this cruise, we recorded the position of the observed bands from the LORAN-C, and the ice band orientation from the S-band radar. The figure shows that we encountered 5 bands during the traverse, the widest of which was 2 km, and that the band spacing varied between 5-10 km. We also observed that the swell was in the wind direction and decreased in magnitude as we moved northwest through the bands. The traverse ended when we encountered ice which was too heavy to steam through; at this point, Pease's station was a further 81 km at 44°T inside of the pack ice. The following day during an overflight to recover her station, Pease found that the pack ice between the ship and the station had the following structure: In the outer 10-20 km, the ice was organized into compact zones of broken ice, which were interspersed with occasional large leads and polynyas, where the leads were approximately oriented at right angles to the wind. Further into the pack, the ice concentration was greater, with many of the small floes refrozen into km-sized aggregates. The leads were sparser and still ran at approximately right angles to the wind. The station was located in a region of high concentration on a floe which was quasi-rectangular and measured about 10 by 20 m.

Figure 9 shows the relative displacement of KURT from Peaset's station. The station was initially 80 km northeast of KURT; we assume that approximately the same tidal currents and winds acted on the two buoys. The figure shows, however, that KURT moves away from the station at a mean speed of  $0.48 \text{ km hr}^{-1}$  or  $0.13 \text{ m s}^{-1}$ , so that the band moves 30% faster than the interior ice. Section 5 shows that

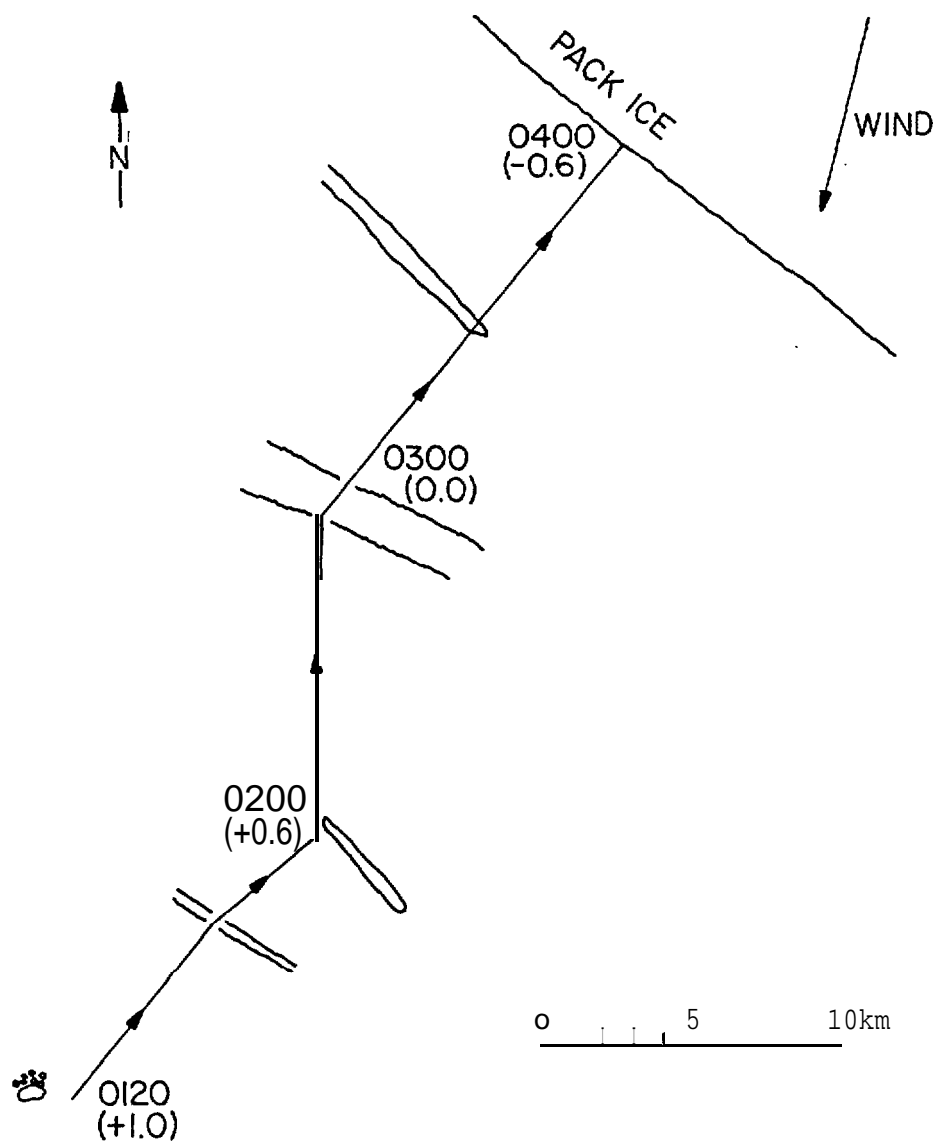


Figure 8. A schematic drawing of the ice features encountered during the return to the ice edge on 10 March, 0100 - 0400 GMT. The solid line shows the cruise trajectory; the adjacent numbers give times in GMT; the numbers in parentheses are the water temperatures in degrees. The arrow shows the mean wind direction; the mean wind speed was  $15 \text{ m s}^{-1}$ .

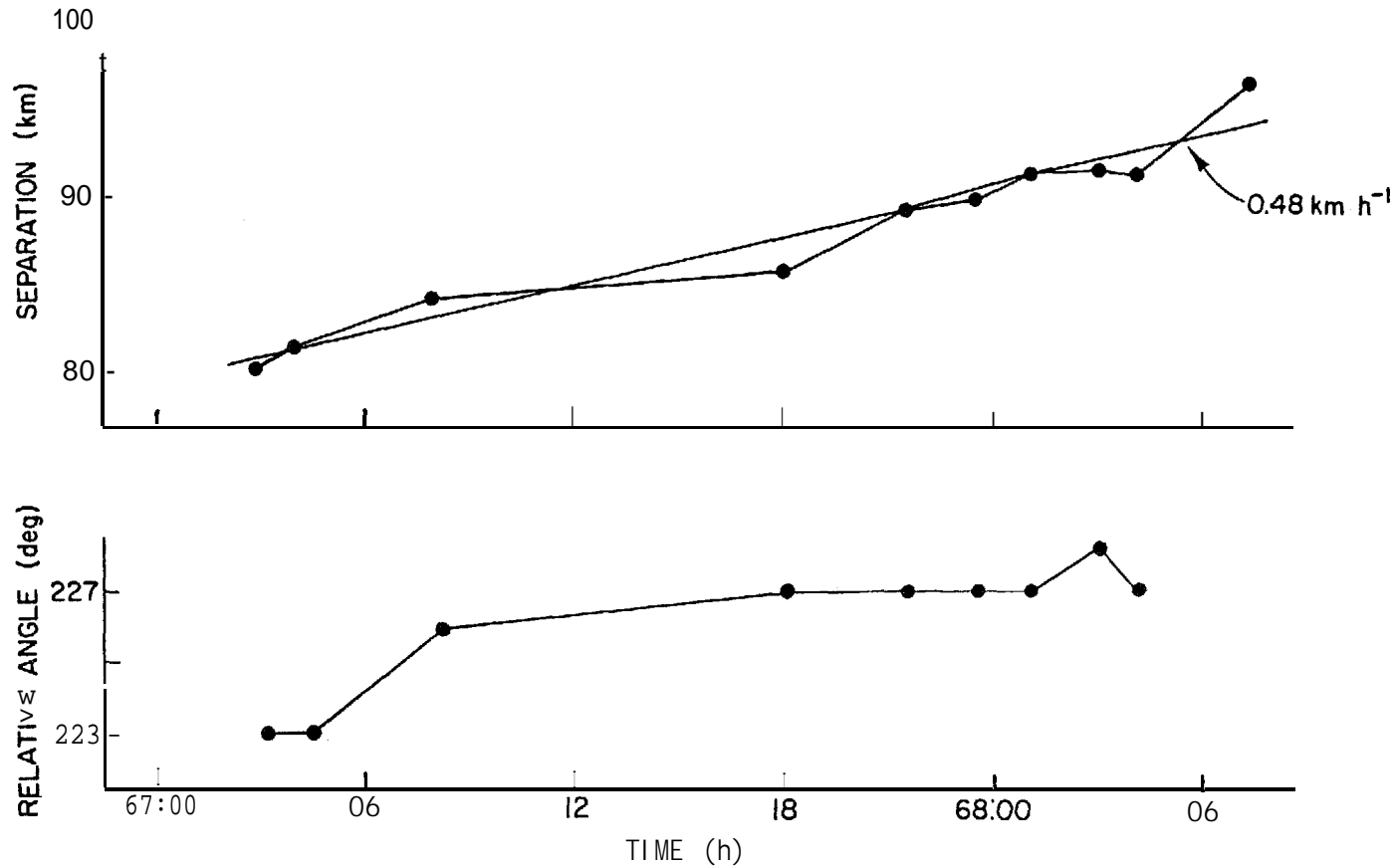


Figure 9. Relative displacement of KURT from Pease's station. The dots show the separation, the solid straight line is a least-squares fit showing that KURT moved away from Pease's station at a speed of  $0.48 \text{ km hr}^{-1}$  or  $0.13 \text{ m s}^{-1}$

the cause of this speed increase is the radiation stress on the band exerted by the wind waves generated in the fetch between the band and the ice margin. Before discussing of the band momentum balance, however, we first discuss how wind-waves contribute to the band structure and erosion.

#### 4. Wave Erosion of the Band

To illustrate first the band structure, Figure 10 is a composite photograph of the cross-section of a small band, made 2 hr after the photograph in Figure 5. As determined from the LORAN-C, the band is approximately 100 m wide. The photograph shows that the band consists of 3 - 5 m diameter floes downwind, with a sharp water-ice boundary at the leading edge. Although it is not apparent on the photograph, the seawater surface downwind of the band is also smooth. In contrast, the ice on the upwind edge is diffuse and consists of small ice pieces which are strongly wave-agitated.

Figure 11, a schematic drawing of a band in cross-section, shows that at the upwind band edge, the wind waves are reflected and absorbed. Further, the wave agitation breaks up the larger floes into small pieces. These small floes then drift upwind relative to the larger floes in the consolidated band for the following reason: For an ice floe to be a good wave reflector, the floe diameter must be greater than half the incident wavelength, so that for the same incident wave, large floes are good reflectors and small floes are bad reflectors. Therefore, the **small** floes experience less of a radiation stress than the large floes so that once the small floes form, they drift upwind relative to the consolidated band. This physical process, where the broken-up floes experience a smaller radiation stress and then drift upwind relative to the band, explains the diffuse nature of the trailing band edge. Because of this process, small floes constantly break off the upwind band edge, drift relatively upwind, and melt in



Figure 10. Composite photograph of a small 100 m wide band; downwind is to the left, upwind is to the right.

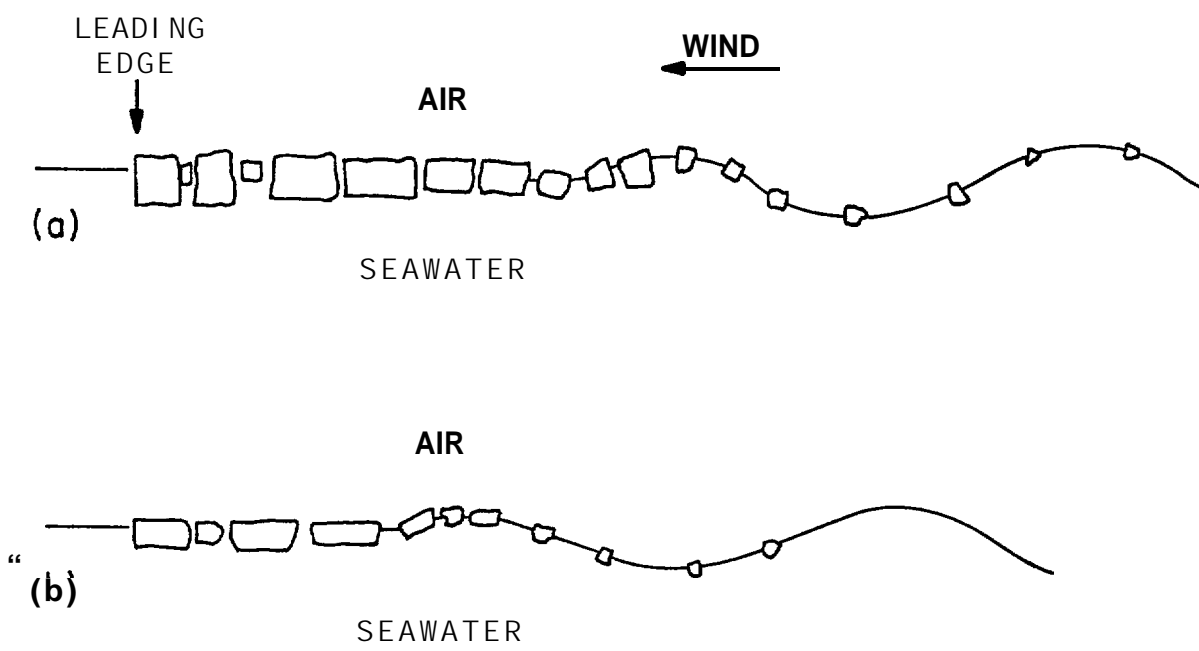


Figure 11. Schematic drawing in cross-section of the evolution of a band in a wave field. (a) Initial band configuration; (b) some time later. See text for additional discussion

the surrounding warm water. The new ice thus exposed to the wind-waves also breaks up, drifts away, and melts so that the erosive process continues. Therefore as Figure 11 shows, the band melts both by **the interior floes** growing thinner in the vertical and by the horizontal erosion of the upwind edge.

For an additional detailed look at this melting process, Figure 12 shows the seawater temperature taken at 1 hr intervals **from the ship** while following the ice band, plotted versus time. The figure shows that the temperature began at the seawater freezing point, then had a nearly step increase of 2 degrees between **1800 - 2400 hr**, 8 March. The following three photographs (Figures 13a, b, c) show details of the deterioration of the upwind band edge **in** the warm seawater following 0000 hr, 9 March (day 68). In Figure 13a the entire band **is visible** with the upwind edge to the right. Although it is not apparent on the photograph, the small floes upwind of the band tend to collect into **Langmuir rolls** formed at right angles to the band. Figure 13b next shows the individual floes upwind of the band, with diameters of 0.2 - 0.3 m; and Figure **13c** shows the small floes well upwind of the band melting **in** the surrounding warm water.

This discussion shows that the wind waves cause the width decrease of the band. For our band, which had an initial width of order **1 km**, and a **final** width of order 50 m, the rate of ice ablation is **on** the order of  $20 \text{ m hr}^{-1}$ . Figures **10** and **11** also show that following **Wadhams** (1982), the wave radiation stress exerts a compressive force which aside from the upwind edge, maintains the band integrity. In the next section, we further show that the radiation stress is of the right magnitude and direction to cause the observed band velocity increase over the ice interior.

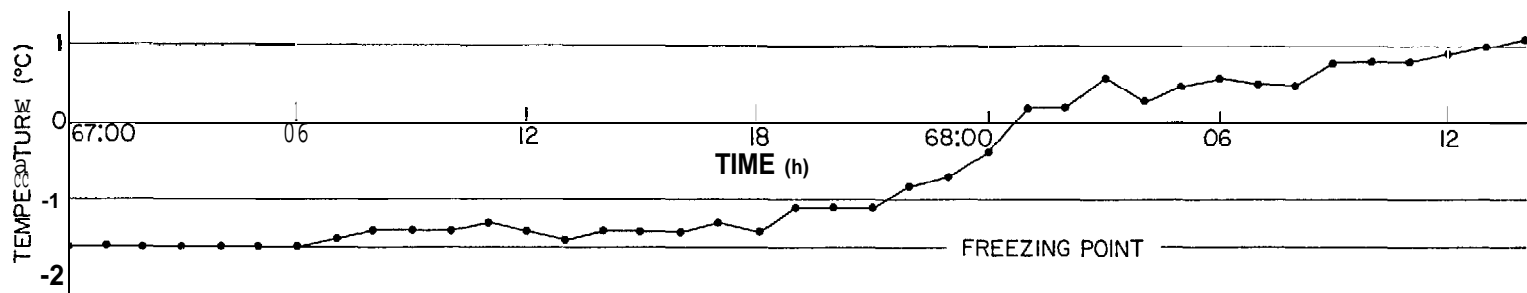
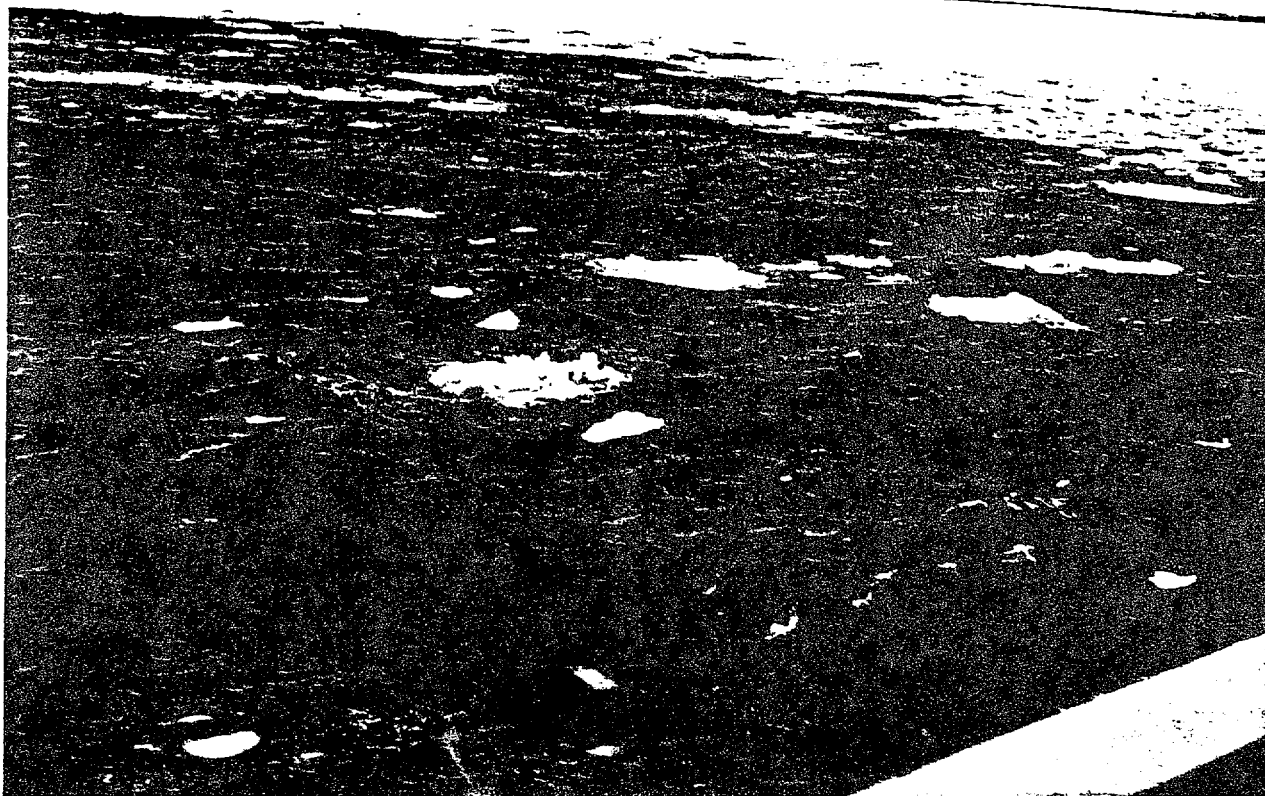


Figure 12. Seawater temperature versus time for the band experiment.



(a)



(b)

Figure 13. Details of an upwind band edge, following 9 March 0000 GMT. (a) The upwind edge; (b) the floes behind the band; (c) small floes melting in open water. See text for further description.



## 5. The Stress Balance on the Band

In this section, we first identify and discuss the terms in the steady momentum balance, then qualitatively show that the tides cause the oscillations on the buoy trajectories, and finally apply the steady momentum balance to the ice band.

In application of the momentum balance, our major uncertainty is regarding water stress. Therefore we derive this stress in two ways: first, through use of the relative velocity observed at the band; second, by a scaling-up of the water stress measured at Pease's station. The use of these two stresses at the band gives a range of additional stress required for the band to move faster than the interior ice. Finally, for bands with widths of the same order as ours, we show that the radiation stress calculated from the observed wind speeds and fetches can account for both the direction and magnitude of the additional stress, so that the radiation stress can cause the increased band velocity.

To model the band motion, McPhee (1979, 1982) gives the following equation for the steady-state momentum balance on an ice floe relative to a **barotropic geostrophic** current:

$$\rho_w \underline{\tau}_w = \rho_a \underline{\tau}_a - i m f \underline{u}_R, \quad (1)$$

where  $\underline{\tau}_w$  and  $\tau$  are respectively the water and air stress,  $\rho_w$  and  $\rho_a$  are the water and air density,  $m$  is the ice density per-unit-area,  $f$  is the Coriolis parameter, and the under-bar denotes a vector. In our analysis, we take  $\rho_a = 1.2 \text{ kg m}^{-3}$  and  $\rho_w = 1030 \text{ kg m}^{-3}$ . The relative ice velocity  $\underline{u}_R$  is given by

$$\underline{u}_R = \underline{u}_I - \underline{u}_G, \quad (2)$$

where  $\underline{u}_I$  is the absolute ice velocity, and  $\underline{u}_G$  is the geostrophic flow due to sea surface tilt.

For the wind stress  $\underline{\tau}_a$ , McPhee uses

$$\underline{F}_a = \rho_a \underline{\tau}_a = \rho_a C_{10} |U_{10}| \underline{U}_{10} \quad (3)$$

where  $C_{10} = 2.7 \times 10^{-3}$ , and  $\underline{U}_{10}$  is the 10 m wind velocity. To simplify our notation, we define  $V = |\underline{u}_R|$ . Then for the water stress, McPhee derives  $\underline{\tau}_w$  from 60 days of summer Beaufort sea ice drift data, for  $0.08 < V < 0.22 \text{ m s}^{-1}$ . . . . McPhee's (1982) best-fit theoretical formulation (his sixth model) gives

$$\tau_w = 0.0128 V^{1.70 \pm 0.00}, \quad (4)$$

and the best fit to his observed data from McPhee (1979) is

$$\tau_w = 0.0104 V^{1.78 \pm 0.12} \quad (5)$$

for  $V$  in  $\text{cm s}^{-1}$ . In both cases,  $\underline{\tau}_w$  is directed in the opposite direction and about  $20^\circ$  to the right of  $V$ .

Before application of the above steady-state momentum balance to the ice band, we first show that the cause of the oscillations in the buoy trajectories is the rotary tidal currents. For simplicity, and because of the close correlation between the two trajectories, we work only with buoy KURT. In this comparison we take the ocean currents from a current meter (BC22) discussed in Muench (1982). Figure 14, a simplified chart of the experimental region, shows the position of the current meter, which was moored at 50 m depth, and the net

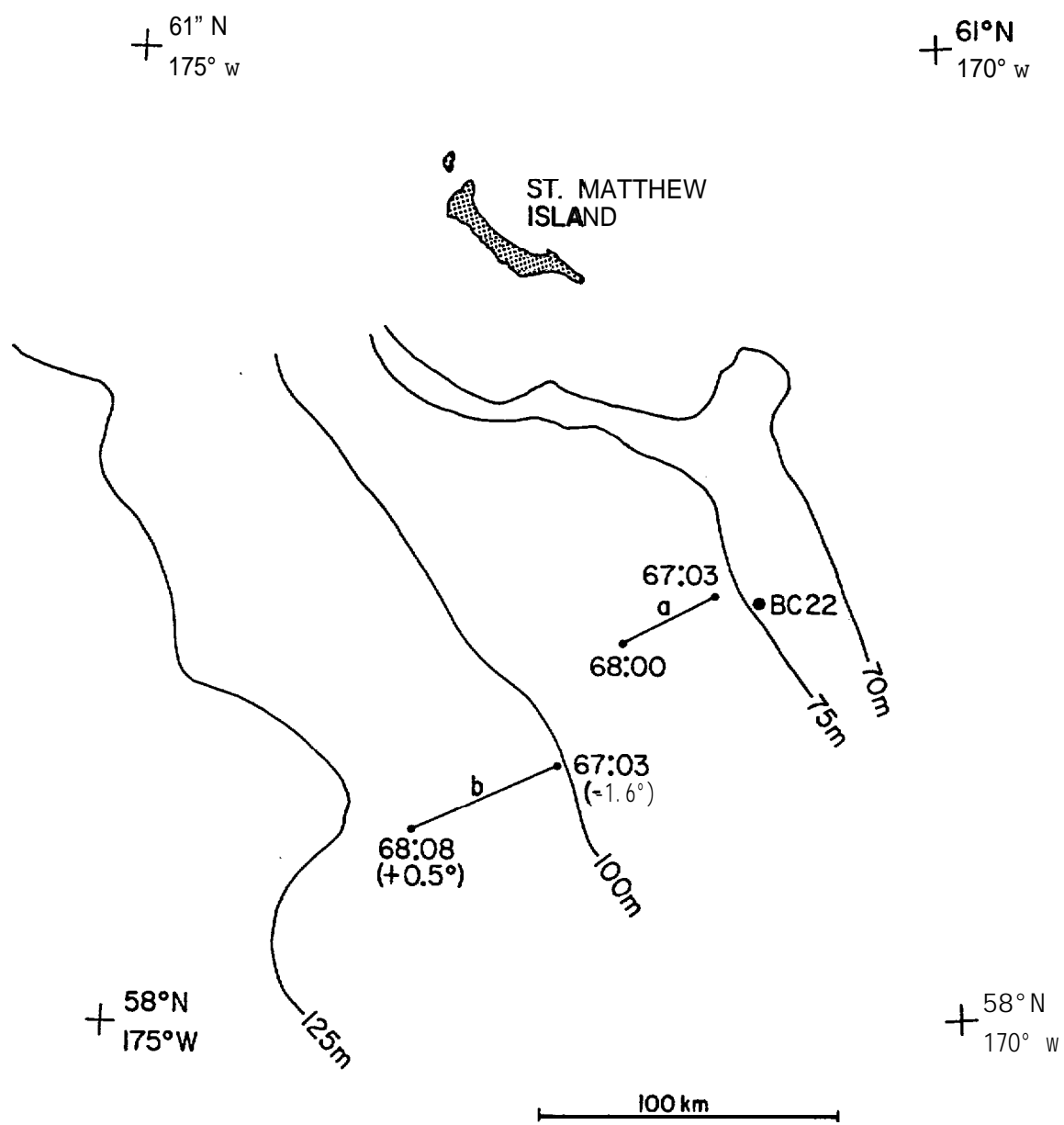


Figure 14. A chart of the experimental region. The point 'BC22' shows the current meter position; the line 'a' shows the net translation of Pease's station for the times shown at the endpoints; line 'b' shows the net band translation. The numbers in parentheses under the times are water temperatures in degrees.

southwest translation of Pease's station on line 'a' and KURT on **line 'b'**, for the times shown at the line endpoints.

The figure shows that the band is between 90 - 140 **km** southwest of BC22 in water depths of 100 - 125 m. From a **CTD** survey during the cruise, **Muench** (1982) shows that the seawater at BC22 is nearly homogeneous, while the rising temperatures along the band trajectory correspond to a 100 km wide region of **two-layered** stratification in both temperature and salinity with an average interface depth of 30 m, with the two-layer structure running approximately parallel to the **isobaths**. Because of the change in depth and oceanic stratification at the band relative to **BC22**, application of the BC22 currents to the band may be complicated by amplitude and phase shifts. Even with these potential **changes, it** can be seen from Figure 15 that the BC22 currents account for most of the oscillations in the band trajectory. On the figure, the top 2 curves show the north  $u_c$  and west  $v_c$  current components from BC22; the middle two curves,  $u_I$  and  $v_I$ , show the ice band velocity components, which are filtered with a 2.5 hr running average; and the lower two curves show the relative velocities  $u_R = u_I - u_c$ . Examination of the lower curves shows that the rotary tide accounts for most of the oscillatory motion on the trajectory. The remaining slight oscillations are either caused by the band position change relative to **BC22**, or by inertial oscillations.

Next, to average out the diurnal and semi-diurnal tides from the band data, and to derive the steady state force balance on the band, we average all relevant quantities over the 25 hr period beginning at 8 March, 0600 **GMT**. For the currents, Table 1 lists the mean components of  $u_I$ ,  $u_c$ , and  $u_R$ . We **assume that the mean current  $u_c$  is** due to the sea surface tilt. Then, using  $|u_R|$  and the wind velocity observed on the ship, we calculate the terms in (1) which make up the steady state stress balance. We then sum these stresses to derive the magnitude and direction of the residual stress  $F_R$ .

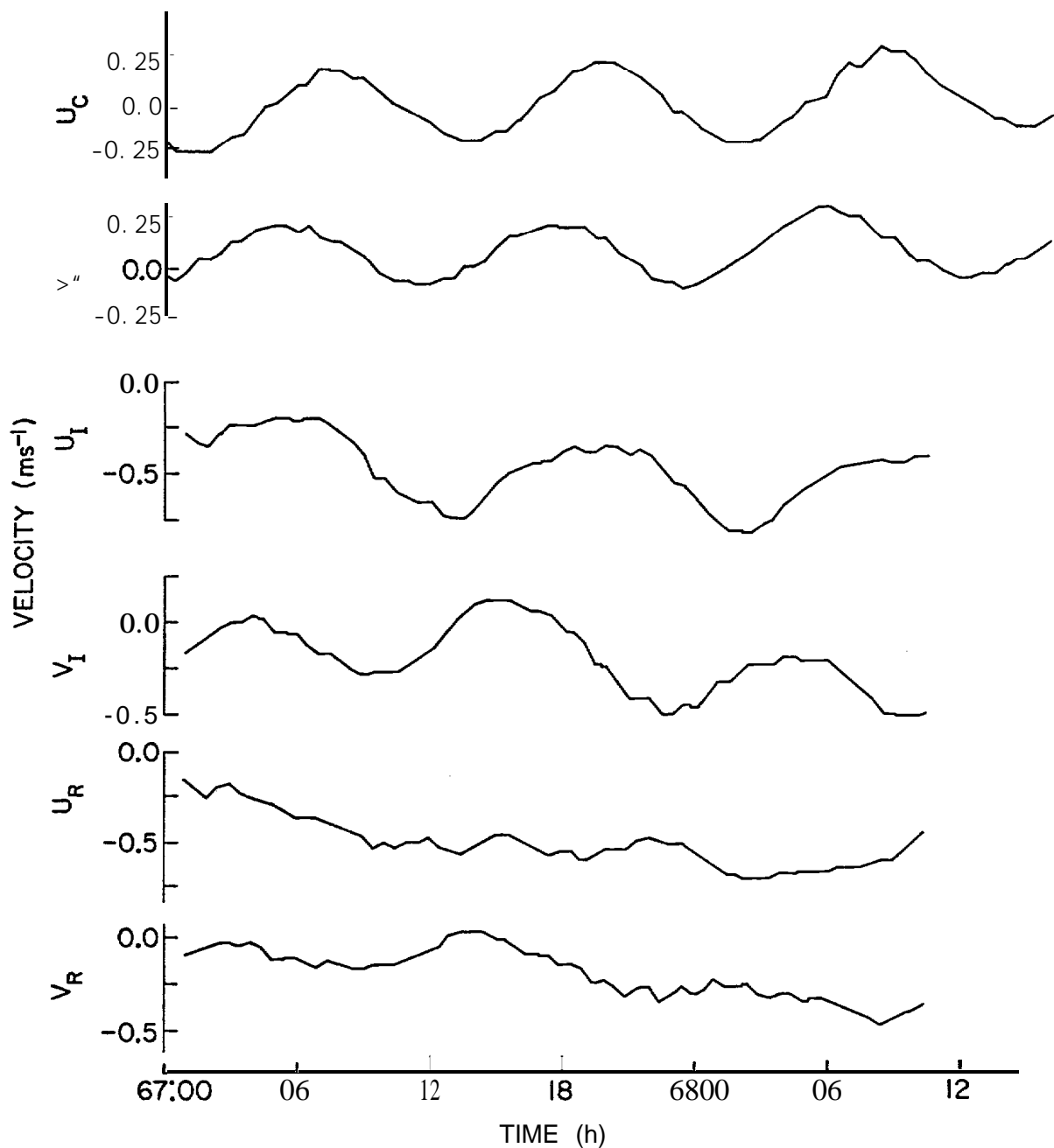


Figure 15. Comparison of the **band** velocity with the currents measured at **BC22**. The upper two curves show the east  $u_C$  and north  $v_C$  current components from **BC22**; the middle two curves show the ice band components  $u_I$  and  $v_I$ ; the lower two curves show the relative velocities  $u_R$  and  $v_R$ . See text for additional description.

Table 1. Average velocities used in the calculation of **the** ice momentum balance.  $\underline{u}_I$ , absolute ice velocity;  $\underline{u}_C$ , currents at **BC22**;  $\underline{u}_R$ , relative ice velocity. 'x' , east direction; 'y' , north direction, 'mag', magnitude, 'deg', current direction in true degrees.

---

velocity	A x	. y	mag	deg
$\underline{u}_I$	-0.529	-0.179	0.56	251°
$\underline{u}_C$	-0.002	+0.093	0.09	359°
$\underline{u}_R$	-0.527	-0.272	0.59	243°

Table 2 lists the **values** of the stresses acting on the band. To calculate the air stress, we use the hourly wind speed and direction shown in Figure 16 as recorded from a cup anemometer and a wind vane mounted on a mast above the bridge. For  $\underline{F}_a$ , we substitute these winds into equation (3), then average (3) over the 25 hr period. To calculate the **Coriolis** stress  $\underline{F}_c$ , we use  $f = 1.25 \times 10^{-4} \text{ s}^{-1}$  corresponding to  $59^\circ \text{ N}$ ,  $m = 1.9 \times 10^3 \text{ kg m}^{-2}$  corresponding to an average ice thickness of 2 m, and the value of  $\underline{u}_c$  given in **Table 1**. To calculate the magnitude of the water stress  $\underline{F}_w$ , we substitute  $V = 59 \text{ cm s}^{-1}$  into equation (4) giving the mean water stress as  $1.34 \text{ N m}^{-2}$ . For the direction of  $\underline{F}_w$  we **follow** the formulation of the sixth drag law in McPhee (1982, Table 1) which gives the stress direction  $\alpha$ , as

$$\alpha = \alpha_2 - 180^\circ - \beta$$

where  $\alpha_2$  is the ice velocity direction, and we calculate  $f$  as  $19^\circ$ . We then use these values to calculate the vector components of  $\underline{F}_w$  listed in Table 2. Finally, the last line in Table 2, which gives the values of  $\underline{F}_R$  necessary to complete the stress balance, shows that  $\underline{F}_R$  has a magnitude of  $0.8 \text{ N m}^{-2}$  in the wind stress direction. The additional stress required for balance then, is both of the same order and in the same direction as the wind stress.

There are several problems with the formulation in Table 2. First, our ice velocity of  $0.59 \text{ m s}^{-1}$  is 2.5 times the largest velocity measured in **McPhee's** field data. This **leads** to a large range of error. For example, substitution of  $0.59 \text{ m s}^{-1}$  into equation (5), which **is** McPhee's least-square best fit empirical equation, gives a stress range of  $0.9 - 2.5 \text{ N m}^{-2}$ . Substitution of these magnitudes alone in the stress balance gives that  $\underline{F}_R$  ranges between  $0.5 - 2 \text{ N m}^{-2}$ . Second, with regard to the wind stress, we felt when the quartermasters measured

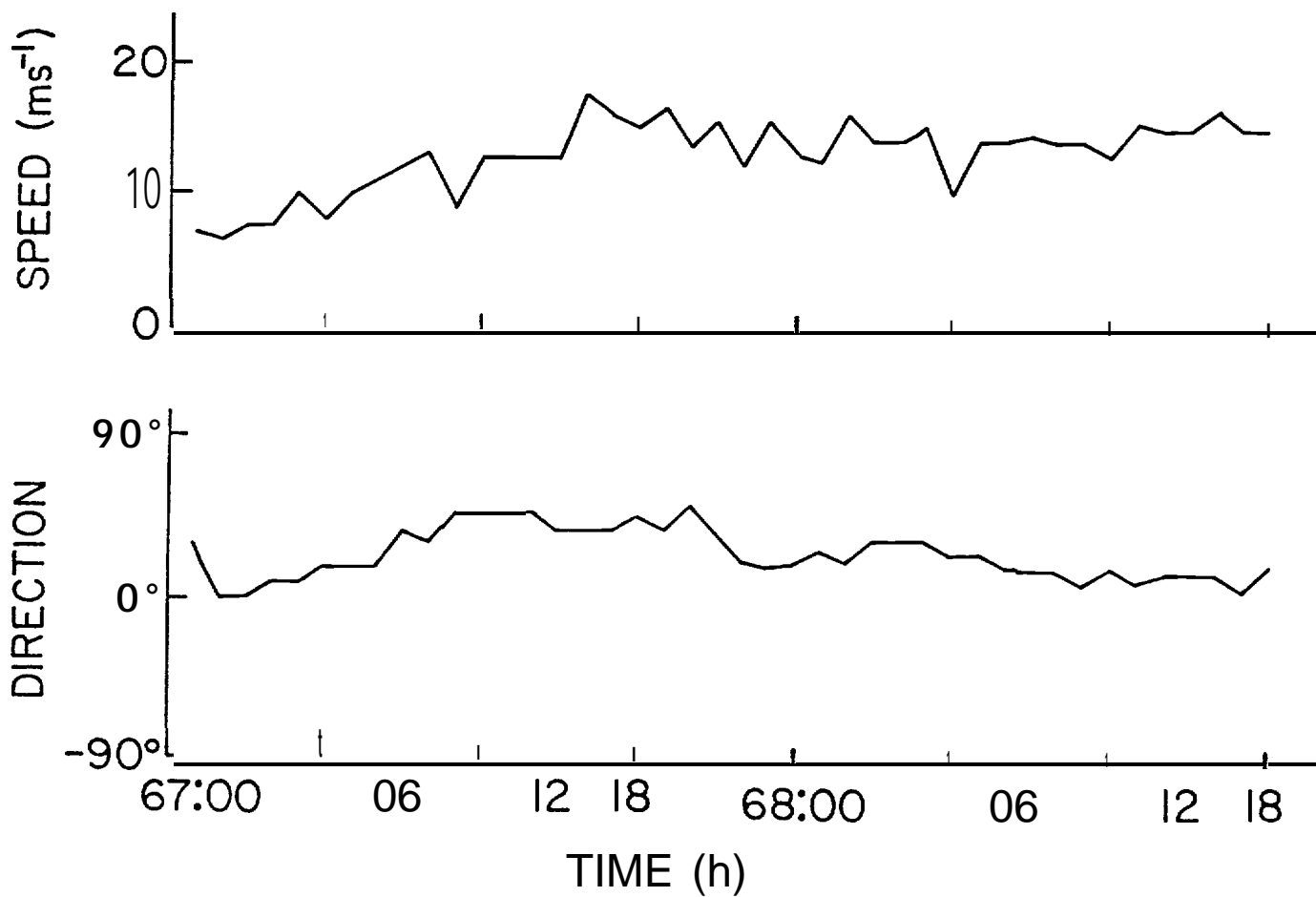


Figure 16. Observed wind speed and direction for the band experiment as measured on the ship at one-hour intervals.

Table 2. Stresses on the ice band.  $F_w$ , water stress;  $F_a$ , air stress;  $F_c$  Coriolis stress;  $F_R$ , residual stress required for balance; all in  $N m^{-2}$ . See caption of Table 1 for notation.

---

Stress	$\hat{x}$	$\hat{y}$	mag	deg
$F_w$	0.93	0.96	1.34	44°
$F_a$	-0.36	-0.49	0.61	216°
$F_c$	-0.06	+0.13	0.14	333°
$F_R$	-0.51	-0.60	0.79	220°

the hourly wind speed on the ship, they underestimated the effect of gusts. An increase of the mean wind speed by 10% yields a 20% increase in the wind stress, which reduces  $\underline{F}_R$  to  $0.6 \text{ N m}^{-2}$ . Finally, our assumption of a 2 m average ice thickness is only an estimate. Reduction of this value from 2 to 1 m, however, only reduces  $\underline{F}_R$  by a negligible amount.

Our second method for calculation of the ice band water stress is to scale up the water stress measured at Pease's station, where the radiation stress is negligible, by the ratio of the band and station velocities raised to the 1.7 power. From her drag and position measurements, Pease calculated for the same 25 hr period the average station velocity and stress balance. First, the relative velocity  $\underline{u}_R^i$  of her station is as follows:

$$\omega_R = -0.37 \text{ m s}^{-1}, \quad \omega_R = -0.27 \text{ m s}^{-1}, \quad (6)$$

or  $v' = 0.45 \text{ m s}^{-1}, \quad a' = 234^\circ,$

where  $V'$  and  $a'$  are the current magnitude and direction. Comparison of the station and band velocities shows that, consistent with Figure 8, the station moves  $0.14 \text{ m s}^{-1}$  slower than the band.

Second, Table 3, which lists the measured stress balance for 1 m thick ice at Pease's station, shows that as a first approximation the air and water stress are in balance. Further the table shows that, although the wind stress at the station approximately equals the wind stress on the band, the station water stress is only 38% of the stress derived for the band. Therefore, an alternative method for calculation of the water stress on the band is to scale up the stress measured at Pease's station by the ratio

Table 3. **Stress** balance at Pease's station. See caption of Table 1 for notation.

---

Stress	$\hat{x}$	$\hat{y}$	mag	deg
$F_w$	0.32	0.38	0.50	400
$F_a$	-0.35	-0.41	0.54	220"
$F_c$	-0.03	+0.04	0.05	324°
$\backslash R$	+0.06	-0.01	0.06	260°

$$\left(\frac{v}{v_1}\right)^{1.7} = 1.58 ,$$

which yields a stress of  $0.8 \text{ N m}^{-2}$  in magnitude acting on the band. Table 4, which lists for this water stress the new band stress balance shows that the residual stress is now  $0.3 \text{ N m}^{-2}$  and still directed approximately in the wind direction. In summary, Tables 2 and 4 show that depending on which method we use for calculation of the water stress,  $F_R$  is in the range  $0.3 - 0.8 \text{ N m}^{-2}$ , and is directed approximately in the wind direction.

We next show that the wind-wave radiation stress can provide  $F_R$ . Following Longuet-Higgins (1977), if the ice band totally absorbs the wave energy with no transmission or reflection, then the radiation stress  $S$  in  $\text{N m}^{-1}$  is

$$S = \frac{1}{4} \rho_w g a^2 = \frac{1}{2} \epsilon \quad (7)$$

where  $g$  is the gravity acceleration  $9.8 \text{ m s}^{-2}$ ,  $a$  is a characteristic incident wave amplitude, and  $\epsilon$  is the incident wave energy density.

Hasselmann et al (1973) give  $\epsilon$  as the following function of fetch  $X$  (in km) and wind velocity  $U_{10}$ :

$$\epsilon = 1.6 \times 10^{-4} \rho_w X U_{10}^2 , \quad (8)$$

so that

$$S = 8.2 \times 10^{-2} X U_{10}^2 . \quad (9)$$

For the same formulation, the dominant wave frequency  $\omega_0$  is given by

Table 4. Recalculation of the stress balance on the ice band, using Pease's water stress **scaled** up from Table 3. See caption of Table 1 for notation.

---

Stress	$\hat{x}$	$\hat{y}$	meg	deg
$F_w$	0.51	0.60	0*79	40°
$F_a$	-0.36	-0.49	0.61	216°
$F_c$	-0.06	<b>+0.13</b>	0.14	333°
$F_R$	-0.09	-0.24	0.26	200°

$$\omega_0 = 2.2 \left[ \frac{g^2}{U_0 X} \right]^{1/3} \quad (10)$$

We next calculate S for the observed range of wind speeds (10-20 m S-1) and fetches (5-10 km). Our choice of fetches is consistent with both Figure 8 and the observations of **Muench** and **Charnell** (1977). Because our unknown in the force balance is the band width, we then use S to calculate the range of band widths for  $F_R = 0.3$  and  $0.8 \text{ N m}^{-2}$ . Table 5 shows the dependence of S on X and  $U_{10}$ , and the resultant band widths. In the table, the first number in each of the four **blocks** is S; the two lower numbers in parentheses are the band widths for the two cases  $0.3$  and  $0.8 \text{ N m}^{-2}$ . To show that for each case the no-transmission assumption is valid, for the case  $X = 10 \text{ km}$  and  $U_{10} = 20 \text{ m s}^{-1}$ , we calculate from equation (10) the dominant frequency  $\omega_0 = 1.7 \text{ s}^{-1}$  which corresponds to a wavelength of 20 m. The general requirement for total reflection of the wave energy from a floe is that the floe diameter be greater than half the incident wavelength. Since our floe diameters are about 10 m, this criterion is met for the longest fetch, highest wind speed case.

The table shows that for total energy absorption, that the band widths range from 0.1 - 1 km. On the further assumption of total wave reflection, all of the widths in the table would be doubled, so that even for  $0.8 \text{ N m}^{-2}$  case, for 10 km of fetch a band made up of deep wide floes can be 1 km wide. We also note that as the bands **move** downwind and thin out by the mechanism described above, the bands **will** begin to transmit the longer incident wavelengths. This leakage of energy through the band will reduce the incident radiation stress and explains why the bands do not continue to accelerate with increasing fetch.

Table 5. Radiation stress ( $N\ m^{-1}$ ) and resultant band widths (m) as a function of fetch X, and wind speed  $U_{10}$ . The top number in each block is the stress; the lower **two** numbers in parentheses are the band widths for the two cases.

---

$X / U_{10} (m\ s^{-1})$ (km)	10	20
5	40 (50, 140)	160 (200, 530)
10	80 (100, 270)	330 (400, 1,100)

## 6. Concluding Remarks

The present study shows that the wind waves account for both a large part of the band decay and the band velocity increase relative to the ice interior. Because the long axes of the bands lie approximately at right angles to the wind, the bands serve as line wave absorbers and reflectors, so that the processes of band decay and acceleration are more efficient than for randomly-oriented bands. The problems which are unsolved include the question of how the bands initially form, the exact nature of the water stress on the bands, and the dependence of the rate of band ablation on wind, waves, and water temperature.

Also, not all bands are linear; some of them occur as complicated sinuous patterns. Figure 17 shows an example of a band observed as we **left** the ice edge on 11 March, 0000 GMT, where the only noticeable ocean waves were from the wind direction. At present, we have no idea as to how these complicated structures form and evolve. In summary, the bands are efficient structures for the absorption and reflection of wave energy where the energy and radiation stress go into increased band velocities and the band ablation. Thus, the ice bands are probably strong contributors to the maintenance of the ice edge position **through** rapid ice export and melting.

## Acknowledgments

We are grateful to Captain Bruce I. Williams and the officers and crew of the NOAA ship SURVEYOR. Without their help and patience, we could never have done this experiment. We **also** thank Carol Pease, for her role as chief scientist, for allowing **us** to use the data from her ice interior station, and for many useful conversations about stress balance. We also thank Dr. Robin **Muench** for the use of his current meter data, John Gunn and Patricia **Fogle** for help with the data processing, Jane Bauer for conversations about radiation stress, **Cathie**

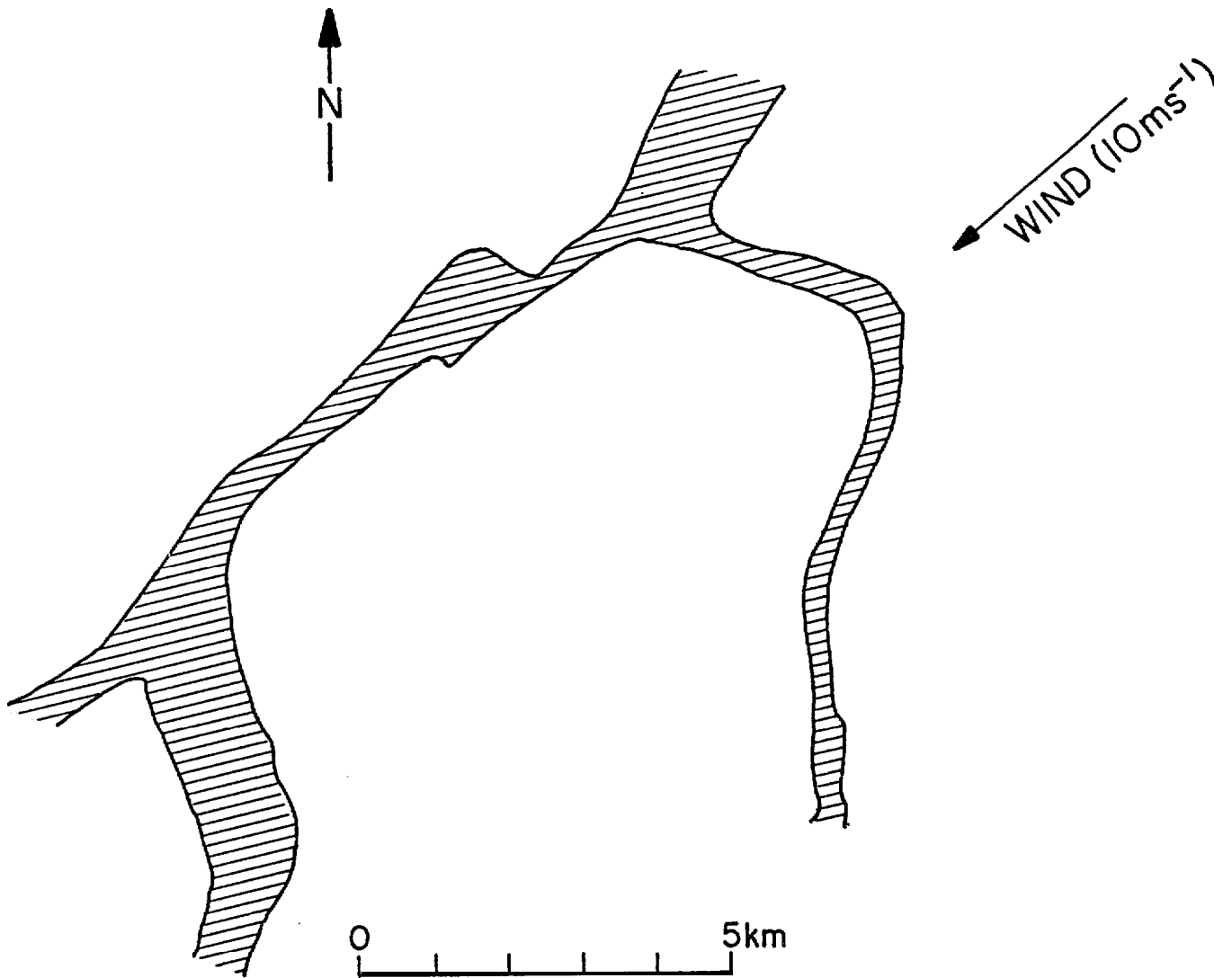


Figure 17. Sketch of ice band made on 11 March 0400 GMT while leaving the ice edge (courtesy Scott **Ferguson**).

**Boyd** for typing this manuscript, Scott Ferguson for providing the sketch shown in Figure 17, and **Jeral Turay** and Kurt **Zaverson** for the loan of their names. **This** work was primarily supported by the **BLM/NOAA** Outer Continental Shelf Program through Contract **NA81RAC000-13**; we are very grateful for their support. **We** also acknowledge the support of the Office of Naval Research under Project NR307-252 and Contract **N00014-76-C-0234**, **which** supported the radar buoy development and the manuscript preparation. This is contribution No. 0000 of the School of Oceanography, University of Washington.

## References

- Bauer, **B.J.** and S. Martin, Field observations of the Bering Sea ice edge properties during March 1979, Mon. Wea. Rev. 108, 2045-2056, 1980.
- Hasselmann, K. et XV al., Measurements of wind wave growth and swell decay during the Joint North Sea Project (JONSWAP), Herausgegeben vom Deutsch. Hydrography. Institut. , Reihe A, no. 12, 95 pp., 1973.
- Longuet-Higgins, M.S., The mean force exerted by waves on floating or submerged bodies with applications to sand bars and wave power machines, Proc. Roy. Soc. Long. A. 352, 463-480, 1977.
- McPhee, M.G., The effect of the oceanic boundary layer on the mean drift of pack ice: application of a simple model, J. Phys. Ocean. 9, 388-400, 1979.
- McPhee, M.G., Sea ice drag laws and simple boundary layer concepts, Rev. Geophys. and Space Phys. (in press), 1982.
- Muench, R.D. and R.L. Charnell, Observations of medium-scale features along the seasonal ice edge in the Bering Sea, J. Phys. Ocean. 7, 602-606, 1977.
- Pease, C.H. S.A. Sale, and J.E. Overland, Drag measurements for first-year sea ice over a shallow sea, J. Geophys. Res. (submitted), 1982.
- Wadhams, P., A mechanism for the formation of ice edge bands, J. Geophys. Res. (submitted), 1982.